ORIGINAL RESEARCH

Infrared Reflection Absorption Spectroscopy of OH Adsorption on the Low Index Planes of Pt

Hiroyuki Tanaka · Seiho Sugawara ·
Kazuhiko Shinohara · Takahiro Ueno ·
Shunsuke Suzuki · Nagahiro Hoshi · Masashi Nakamura

Abstract The adsorption of hydroxide (OH_{ad}) on Pt has been studied on the low index planes of Pt using infrared reflection absorption spectroscopy (IRAS) in electrochemical environments. We discuss the correlation between the integrated band intensity of the bending mode of OH of Pt–OH (δ_{PtOH}) and the charge density of the oxide formation of Pt. The band of δ_{PtOH} is observed around 1100 cm^{-1}, and the onset potential depends on the surface structure. The onset potential of δ_{PtOH} on Pt(110) and Pt(100) overlaps with the hydrogen adsorption/desorption potential region. The order of the integrated band intensity of δ_{PtOH} at 0.9 V vs RHE is opposite to the order of the oxygen reduction reaction (ORR) activity. This finding supports that the OH_{ad} is one of the species deactivating the ORR.

Keywords IRAS · Electrochemical environments · Adsorption of hydroxide · Oxygen reduction reaction

Introduction

Polymer electrolyte fuel cells (PEFCs) are expected to be useful power generation systems and automotive power sources because the efficiency of energy conversion is high. However, there are many issues related to use of the PEFCs

H. Tanaka · T. Ueno · S. Suzuki · N. Hoshi (✉) · M. Nakamura (✉)
Department of Applied Chemistry and Biotechnology, Graduate
School of Engineering, Chiba University, 1-33, Yayoi-cho, Inage-ku,
Chiba, 263-8522, Japan
e-mail: hoshi@faculty.chiba-u.jp
e-mail: mnakamura@faculty.chiba-u.jp

H. Tanaka · S. Sugawara · K. Shinohara
EV System Laboratory, Nissan Research Center, Nissan Motor Co.,
Ltd., 1, Natsushima-cho, Yokosuka-shi, Kanagawa 237-8523, Japan

that must be solved for the wide application. One major issue is the reduction of Pt loading in the catalysts because of the high cost and the limited natural resources of Pt. Enhancement of the activity for the oxygen reduction reaction (ORR) is the most important subjects for the reduction of Pt loading.

Previous papers show that Pt oxides are one of the blocking species of the ORR on Pt electrodes [1, 2]. Therefore, enhancement of the tolerance to the oxide formation is expected to enhance the ORR activity. Surface oxidation of Pt electrodes has been studied using single-crystal electrodes. Pt oxides on Pt(100) and Pt(110) are formed at more negative potentials than those on Pt(111) [3, 4]. Studies using chronoamperometry and voltammetry suggest that adsorbed hydroxide (OH_{ad}) on Pt(111) is formed from the dissociation of water and the $PtOH_{ad}$ is oxidized to PtO at higher potentials [5, 6]. On formation of Pt oxide has been studied using spectroscopic methods under ultrahigh vacuum (UHV) [4, 7–12].

There is no guarantee that Pt oxides prepared in UHV are reproduced in electrochemical environments, because the experimental conditions (pressure, temperature, hydration state, and potential) differ remarkably. Therefore, direct observation of Pt oxides is necessary to understand the oxidation process in electrochemical environments.

We recently reported OH adsorbed on Pt(111) in alkaline electrolyte using improved infrared reflection absorption spectroscopy (IRAS) [13]. In this paper, the adsorption process of hydroxide (OH_{ad}) has been studied on the low index planes of Pt in acid electrolyte using this method. The onset potential of OH_{ad} formation depends on the surface structures. We discuss the influence of OH_{ad} on the ORR activity.

Experimental

A single crystal bead of Pt was prepared from Pt wire (1 mm φ, 99.99 %, Tanaka Kikinzoku Kogyo) in reference to

previous reports [14, 15]. Larger surface area is necessary for the measurement of IRAS spectra with a good signal to noise ratio. We melted the lower half of the bead with an H_2/O_2 flame, added platinum melt from another wire little by little, and finally obtained a large-single crystal in teardrop shape with a cross-sectional area between 0.27 and 0.40 cm^2 [15]. The crystal was oriented using the reflection beam of He–Ne laser from (111) and (100) facets on the bead [15]. Polished Pt single crystal was annealed in H_2/O_2 flame and cooled in Ar/H_2 atmosphere for obtaining atomically flat surface. The annealed surface was protected with ultrapure water and transferred to the electrochemical cell for each measurement.

Cyclic voltammograms were measured in Ar-saturated 0.5 M H_2SO_4 to confirm the crystal orientation. IRAS spectra were measured in 0.1 M HF instead of $HClO_4$ because F^- is invisible in IR light. ClO_4^- has an absorption band around 1100 cm^{-1} that will overlap with the band of OH bending mode of Pt–OH_{ad}. HF solution was prepared with 48.0 % HF (Ultrapur, Kanto Kagaku) and ultrapure water. Cyclic voltammograms in HF are identical with those in $HClO_4$ [4]. The IR light was incident through a BaF_2 prism beveled at 60°. IRAS electrochemical cell was attached to FTIR spectrometer (Bruker Vertex) with a liquid-nitrogen-cooled mercury cadmium telluride (MCT) detector. The prism was covered with a polypropylene thin film (Chemplex Industries) to prevent the dissolution of BaF_2 window. The dissolution of Ba causes the formation of BaOH. The interaction of Ba^{2+} with OH perturbs vibrational state of adsorbed OH [13]. Water was intercalated into the airspace between the polymer thin film and the prism to compensate for the difference in refractive index [13]. Since the thickness of the electrolyte layer between the electrode and the film is a few micrometers, this thin film does not affect the interfacial environment between the electrolyte and electrode. A 1600-cm^{-1} low-pass filter was used for the measurement of OH_{ad}. The spectra were collected with p-polarized light at a resolution of 4 cm^{-1} and were averaged over 1280 scans using subtractively normalized interfacial FTIR spectroscopy (SNIFTIRS). The reference potential was 0.10 V vs RHE, whereas sample potential was changed between 0.20 and 1.20 V vs RHE.

Results and Discussion

Voltammograms of the low index planes of Pt were measured in Ar-saturated 0.5 M H_2SO_4 to confirm the crystal orientation (Fig. 1). The voltammograms were identical with those reported previously [14, 16–19]. Voltammogram of Pt(111) shows sharp redox peaks at 0.47 V, which are assigned to order/disorder phase transition of adsorbed sulfate anion. The adsorption of sulfate anion on Pt(100) and Pt(110) is concurrent with the desorption of H_{UPD} at 0.37 and 0.15 V, respectively [20]. Figure 2 shows voltammograms of the low index planes of Pt in 0.1 M HF. These voltammograms are not symmetrical because the surfaces are roughened by sweeping potential up to 1.2 V. This roughening causes cathodic peak around 0.25 V in the voltammogram of Pt(111) according to the report by Berna et al. [21]. Voltammograms between 0.05 and 0.8 V (not shown here) give no peak derived from the species of glass dissolution and chloride ion contamination. Voltammogram of Pt(111) gives sharp redox peaks at 0.8 V, which are assigned to adsorption/desorption of OH. There has been, however, no direct evidence of PtOH formation in electrochemical environments using insitu methods. We try to observe PtOH band directly using IRAS.

The anodic and cathodic peaks above 0.6 V are related to the formation and reduction of Pt oxides, respectively. The onset potentials of the oxide film formation on Pt(111), Pt(100), and Pt(110) are 0.6, 0.5, and 0.8 V, respectively.

Figure 3 shows the potential dependence of IRAS spectra on the low index planes of Pt. IRAS spectra give a monopolar band around 1100 cm^{-1} on all the electrodes. A previous EELS study reported that PtOH bending mode (δ_{PtOH}) of OH_{ad} on Pt(111) appears around 1015 cm^{-1} [7]. In aqueous solution, the δ_{PtOH} band shifts to a higher frequency due to the formation of hydrogen bonding between hydrated water and OH_{ad} [13]. In deuterated water, this band is not observed
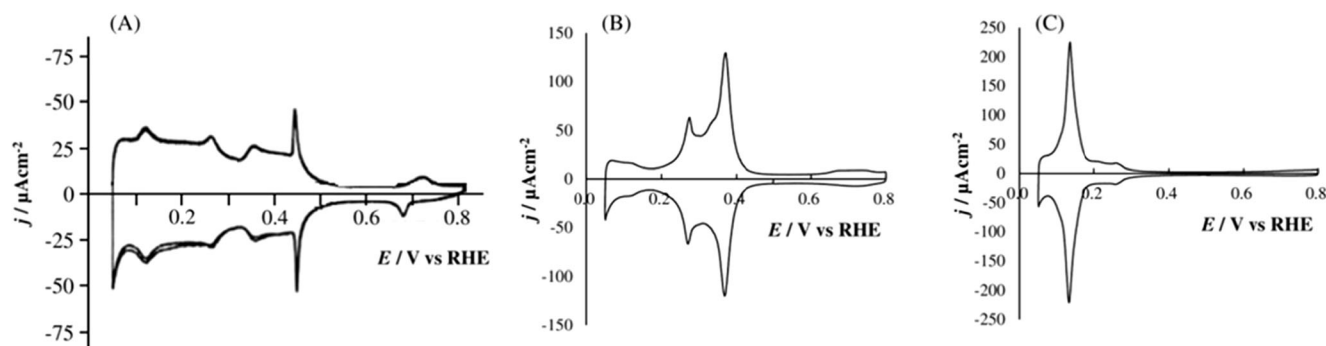
**Fig. 1** Cyclic voltammograms in 0.5 M H_2SO_4 with 50 mV s^{-1} of **a** Pt(111), **b** Pt(100), and **c** Pt(110)
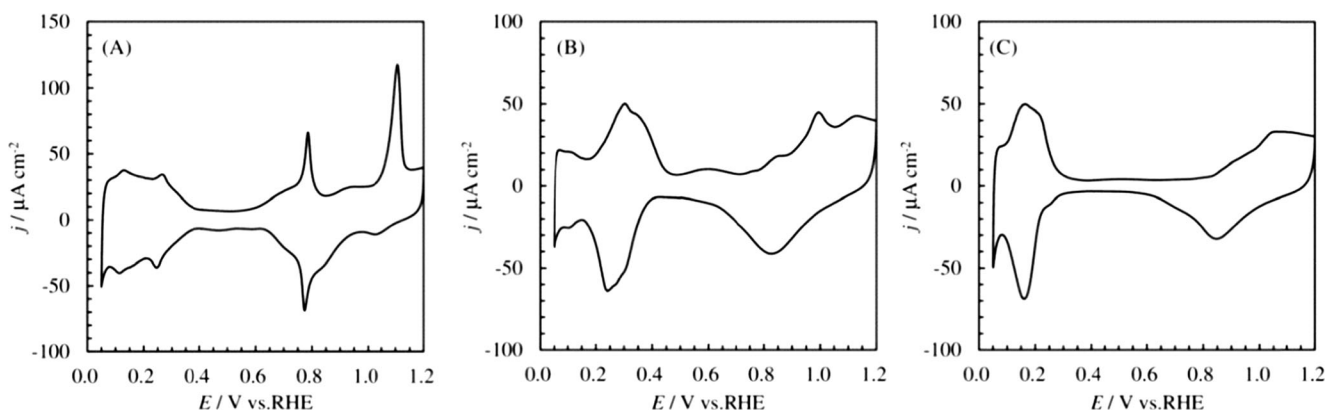
**Fig. 2** Cyclic voltammograms in 0.5 M HF with 50 mV s^{-1} of **a** Pt(111), **b** Pt(100), and **c** Pt(110)

above 900 cm^{-1} due to the isotope shift [13]. Therefore, the bands around 1100 cm^{-1} can be assigned to the δ_{PtOH} of OH$_{ad}$ on Pt. The increase of the band intensity indicates the increase of the coverage of OH$_{ad}$ at positive potentials. The full width at half maximum of the band on Pt(100) is wider than that on Pt(111). On Pt(110), the band is split at negative potentials. This structural effect on OH$_{ad}$ is caused by the structural difference of adsorbed layer. In UHV condition, coadsorbed layer of H$_2$O + OH on Pt(111) forms well-ordered structure due to stable hydrogen bonding configuration [10]. On the other hand, the surface symmetries of Pt(100) (fourfold

symmetry) and Pt(110) (twofold symmetry) do not fit well with those of the two-dimensional hydrogen bonding network of H$_2$O + OH layer. The inhomogeneous hydrogen bonding in H$_2$O + OH layer may result in the band splitting and broadening. The spectra above 1300 cm^{-1} are not shown because the absorption of polypropylene film is too strong.

Figure 4 shows the correlation between the integrated band intensity of δ_{PtOH} and the charge of the Pt oxide formation in the voltammogram of Pt(111). The integrated band intensity was estimated by the subtraction of a linear baseline between 950 and 1150 cm^{-1}. The onset potential of δ_{PtOH} band is 0.50 V, which is lower than that of the anodic current in the oxide film formation region of the voltammogram. The onset potential of δ_{PtOH} on Pt(100) and Pt(110) overlaps with the hydrogen adsorption/desorption potential region as described below, whereas the onset potential of δ_{PtOH} on Pt(111) does not overlap with the hydrogen adsorption/desorption potential region. Gibbs thermodynamics study by Garcia-Areaz et al. suggests that the OH on Pt(111) is adsorbed in the double-layer region [22]. XPS study by Wakisaka et al. showed that the onset potential of OH on the low index planes of Pt is
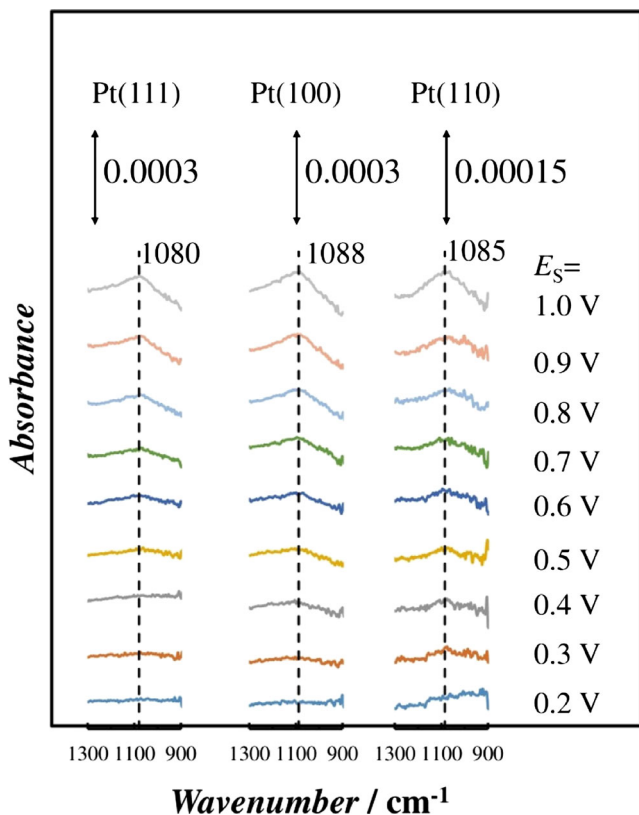
Fig. 3 Potential dependence of IRAS spectra of the low index planes of Pt in 0.1 M HF saturated with Ar. Reference spectra are collected at 0.10 V vs RHE
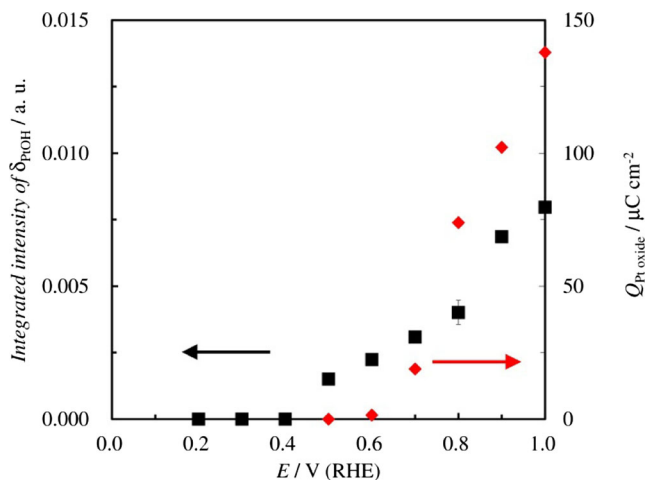
Fig. 4 Correlation between the integrated intensity of δ_{PtOH} (*square*) and the charge of the Pt oxide formation in cyclic voltammogram of Pt(111) (*diamond*)

higher than 0.6 V [9]. This difference between thermodynamics study and XPS study is shown because XPS was measured in UHV condition. In acid solution, OH_{ad} is produced on Pt electrodes as follows [9]:

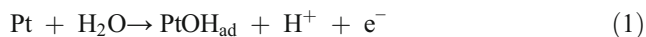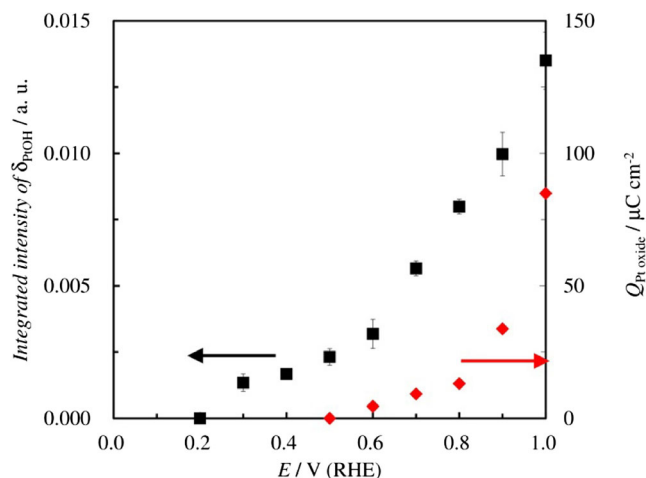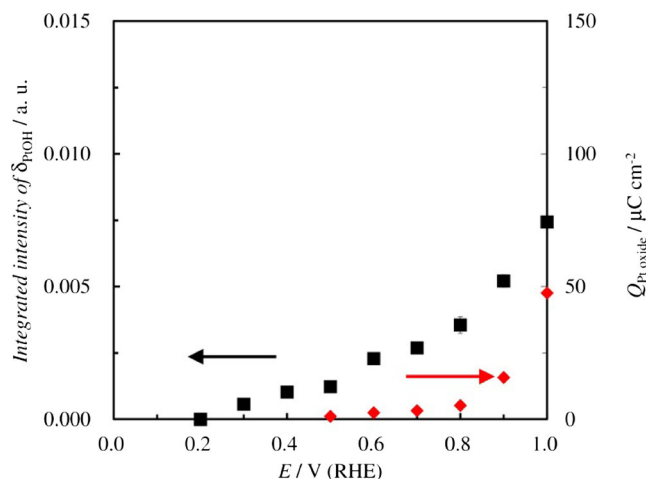$$Pt \ + \ H_2O \rightarrow PtOH_{ad} \ + \ H^+ \ + \ e^- \qquad (1)$$

Figure 5 shows the correlation between the integrated band intensity of δ_{PtOH} and the charge of the Pt oxide formation in the cyclic voltammogram of Pt(100). The onset potential of the Pt oxidation charge is 0.5 V, while the band of δ_{PtOH} appears above 0.3 V. The onset potential of the band on Pt(100) is lower than that of Pt(111). The redox peaks are observed around 0.3 V on Pt(100), as shown in Fig. 2. They are assigned to the peaks due to hydrogen adsorption/desorption reactions. However, the onset potential of δ_{PtOH} band locates in the hydrogen adsorption/desorption region of the voltammogram. This result supports the reports by Garcia-Areaz et al. [22], Gomez et al. [5, 6], and Wakisaka et al. [4]: the OH adsorption potential on Pt(100) overlaps with the hydrogen adsorption/desorption potential, and the redox peaks around 0.3 V include the faradaic current of PtOH formation. Although the charge of Pt oxidation increases steeply above 0.6 V, the integrated band intensity of δ_{PtOH} increases linearly above 0.8 V in Fig. 4. These results indicate that the formation of the oxide species with higher oxidation number such as PtO dominates the oxidation charge above 0.8 V.

Figure 6 shows the correlation between the integrated band intensity of δ_{PtOH} and the charge of the Pt oxide formation on Pt(110). The voltammogram shows that Pt oxides are formed above 0.8 V, while the band of δ_{PtOH} appears above 0.2 V. OH
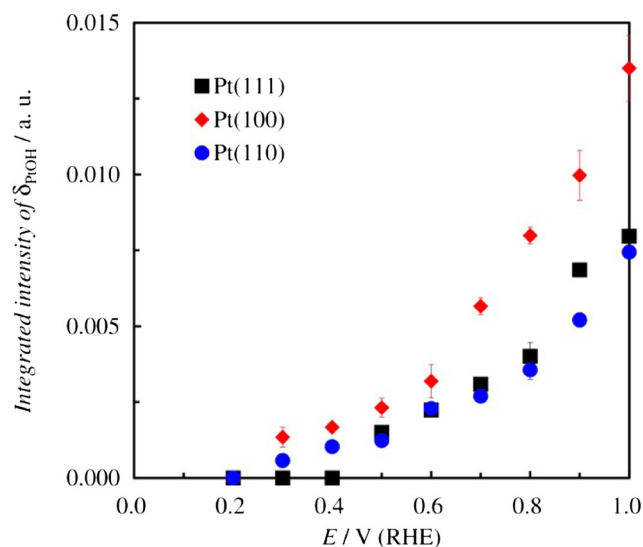

Fig. 6 Correlation between the integrated intensity of δ_{PtOH} (square) and the charge of the Pt oxide formation in cyclic voltammogram (diamond) of Pt(110)

adsorption potential overlaps with that of the hydrogen adsorption/desorption, as is the case of Pt(100).

Figure 7 shows the potential dependence of the integrated band intensity of δ_{PtOH} on Pt(111), Pt(100), and Pt(110). IRAS measurements of each surface orientation were carried out three times using different size of electrodes. The band intensity at each potential was reproduced within the error of 25 %. The absorbance of spectroscopic measurements is proportional to absorption coefficient, optical path length, and concentration according to the Lambert-Beer's low. In IRAS measurement, the band intensity also depends on the incident angle of IR light and the orientation of adsorbed species. Since neither water nor HF absorbs IR light around 1100 cm^{-1}, thickness of a thin layer between electrode and prism does not affect the band intensity of OH_{ad} at a constant incidence angle. DFT calculations predict the most stable structure of

Fig. 5 Correlation between the integrated intensity of δ_{PtOH} (square) and the charge of the Pt oxide formation in cyclic voltammogram (*diamond*) of Pt(100)

Fig. 7 Potential dependence of the integrated band intensity of δ_{PtOH} on the low index planes of Pt in 0.1 M HF

OH$_{ad}$ that is adsorbed at the Pt atop site with Pt–O axis perpendicular to surface. Therefore, *the band intensity of δ-PtOH measured at the same cell geometry will be proportional to the coverage of OH$_{ad}$. The onset potential of δ_{PtOH} band depends on surface structure: Pt(110) < Pt(100) < Pt(111). Pt–OH$_{ad}$ is formed in the hydrogen adsorption/desorption region on the Pt(100) and Pt(110). The integrated band intensity of δ_{PtOH} on Pt(100) is the largest at all the potentials, whereas the integrated intensity on Pt(110) is the smallest above 0.7 V.*

Platinum oxides affect the ORR activity [1, 2]. The ORR activity is estimated by a kinetic current density at 0.9 V vs RHE in many papers. The ORR activity increases as Pt(111) < Pt(100) < Pt(110) in 0.1 M H$_2$SO$_4$ and Pt(100) < Pt(111) < Pt(110) in 0.1 M HClO$_4$ [23–25]. The low activity of Pt(111) in H$_2$SO$_4$ is due to strongly adsorbed (bi)sulfate anions [20]. In our IRAS measurement, 0.1 M HF was used as an electrolyte, since F$^-$ is not adsorbed on Pt electrodes. Voltammograms of Pt single-crystal electrodes in HF are similar to those in HClO$_4$ [4, 23–25]. Therefore, we can correlate the ORR activity in 0.1 M HClO$_4$ with the δ_{PtOH} band intensity in 0.1 M HF. Integrated band intensity of δ_{PtOH} at 0.9 V is as follows: Pt(110) < Pt(111) < Pt(100). This order is opposite to that of the ORR activity.

The ORR activity depends on the geometrical and electronic structure of substrate. There are many deactivation factors of the ORR, such as surface oxidation, impurities, adsorbed anion, and so on. The results above show that the formation of OH$_{ad}$ is one of the deactivation factors of the ORR.

Conclusions

OH bending mode of Pt–OH$_{ad}$ (δ_{PtOH}) has been detected on the low index planes of Pt in 0.1 M HF using in situ IRAS measurement. The onset potential of δ_{PtOH} gets higher as Pt(110) < Pt(100) < Pt(111). Pt–OH$_{ad}$ is formed in the adsorbed hydrogen region on Pt(100) and Pt(110). The integrated band intensity of δ_{PtOH} increases at 0.9 V vs RHE as follows: Pt(110) < Pt(111) < Pt(100). This order is opposite to that of the ORR activity, indicating that Pt–OH$_{ad}$ is one of the deactivation factors of the ORR.

References

1. S. Sugawara, K. Tsujita, S. Mitsushima, K. Shinohara, K. Ota, Electrocatal **2**, 60 (2011)
2. N.M. Markovic, H.A. Gasteiger, B.N. Grgur, P.N. Ross, J. Electroanal. Chem. **467**, 157 (1999)
3. B.E. Conway, G. Jerkiewicz, J. Electroanal. Chem. **339**, 123 (1992)
4. M. Wakisaka, Y. Udagawa, H. Suzuki, H. Uchida, M. Watanabe, Energy Environ. Sci. **4**, 1662 (2011)
5. A.M. Gómez-Marín, J.M. Feliu, Electrochim Acta **104**, 367 (2013)
6. A.M. Gómez-Marín, J. Clavilier, J.M. Feliu, J. Electroanal. Chem. **688**, 360 (2013)
7. G.B. Fisher, B.A. Sexton, Phys. Rev. Lett. **44**, 683 (1980)
8. M. Peuckert, F.P. Coenen, H.P. Bonzel, Electrochim. Acta **29**, 1305 (1984)
9. M. Wakisaka, H. Suzuki, S. Mitsui, H. Uchida, M. Watanabe, Langmuir **25**, 1897 (2009)
10. K. Bedurftig, S. Völkening, Y. Wang, J. Wintterlin, K. Jacobi, G. Ertl, J. Chem. Phys. **111**, 11147 (1999)
11. A.P. Seitsonen, Y. Zhu, K. Bedurftig, H. Over, J. Am. Chem. Soc. **123**, 7347 (2001)
12. G.S. Karlberg, F.E. Olsson, M. Persson, G. Wahnström, J. Chem. Phys. **119**, 4865 (2003)
13. M. Nakamura, Y. Nakajima, N. Hoshi, H. Tajiri, O. Sakata, ChemPhysChem **14**, 2426 (2013)
14. J. Clavilier, R. Faure, G. Guinet, R. Durand, J. Electroanal. Chem. **107**, 205 (1980)
15. N. Hoshi, A. Sakurada, S. Nakamura, S. Teruya, O. Koga, Y. Hori, J. Phys. Chem. B **106**, 1985 (2002)
16. A.M. Funtikov, U. Linke, U. Stimming, R. Vogel, Surf. Sci. **324**, L343 (1995)
17. M.S. Wilson, J.A. Valerio, S. Gottesfeld, Electrochim. Acta **40**, 355 (1995)
18. R. Gomez, J. Clavilier, J. Electroanal. Chem. **354**, 189 (1993)
19. N. Hoshi, T. Suzuki, Y. Hori, J. Phys. Chem. B **101**, 8520 (1997)
20. N.M. Markovic, P.N. Ross Jr., Surf. Sci. Rep. **45**, 117 (2002)
21. A. Berná, J.M. Feliu, L. Gancs, S. Mukerjee, Electrochem. Commun. **10**, 1695 (2008)
22. N. Garcia-Araez, V. Climent, J.M. Feliu, J. Electroanal. Chem. **649**, 69 (2010)
23. N.M. Markovic, H.A. Gasteiger, P.N. Ross Jr., J. Electrochem. Soc. **144**, 1591 (1997)
24. N.M. Markovic, R.R. Adzic, B.D. Cahan, E.B. Yeager, J. Electroanal. Chem. **377**, 249 (1994)
25. J. Perez, H.M. Villullas, E.R. Gonzalez, J. Electroanal. Chem. **435**, 179 (1997)